Journal of Materials Chemistry C

ROYAL SOCIETY OF CHEMISTRY

PAPER

View Article Online
View Journal | View Issue

Cite this: J. Mater. Chem. C, 2022, 10, 14722

Investigation of solution-based synthesis of non-toxic perovskite materials using Mg, Ca, Mn, Fe, Cu, and Zn as the B-site cation for photovoltaic applications†

S. R. Pering, *[a] H. Gillions,[a] T. Kuznetsov,[a] W. Zhang,[a] K. Yendall[b] and M. Togay[c]

Received 20th June 2022,
Accepted 7th September 2022

DOI: 10.1039/d2tc02582e

rsc.li/materials-c

High-efficiency perovskite solar cells are reliant on lead-based materials, which causes toxicity issues for large-scale implementation. Current alternatives can contain similarly environmentally dangerous chemicals such as tin halide compounds. Computational studies have suggested a large array of different potential B-site metal cations that could produce suitable perovskite materials. In this work, simple, solution synthesis of 24 candidate materials is attempted with a focus on the environmental safety of the starting compounds. Of these 24 materials, 10 formed a new material from XRD characterisation, and 1 of the resulting films produces a material with an observable band-gap in UV/vis. This material, a combination of potassium bromide and copper bromide, failed to produce a solar cell of any notable efficiency. This work demonstrates that completely environmentally benign perovskite materials may require more energy-intensive synthesis such as solid-state methods, removing the benefits of simple, solution processing evident in lead-halide perovskite solar cells.

Introduction

To achieve ambitious clean energy targets, the scale of renewable energy implementation needs to increase dramatically. Solar power is a key tool for cutting carbon usage; it has increasingly low energy-payback times, and can be used both in small-scale (household) or large-scale (solar farm) operations. Perovskite solar cells (PSC) are a potentially disruptive technology that has generated significant interest in the relatively short time since their invention.[1] The starting materials for the absorber layer are abundant and the materials themselves can be solution processed, adding ease to scalability.[2–5] Furthermore through simple additions to the original material, methylammonium lead iodide (MAPI), at either the A, B or X-site, the structure of the perovskite can be altered to for example: change the band gap using small ions such as Br^- or Rb^+,[6,7] or; improve the structural integrity of the perovskite through larger additives such as guanidinium or azetidinium.[8–10] Longer chain organic molecules such as 5-ammonium valeric acid can break the 3D perovskite into a vastly more stable 2D structure.[11–14] Combinations of small ion additives can boost the efficiency further, leading to record efficiencies of over 25%.[15]

However the toxic element lead has remained a constant requirement for high-performance cells, and is thus a problem to the widespread application of this technology – particularly with the perovskite's current lack of long-term stability.[16–18] Despite the small amounts of lead present in the thin absorber layer, potential leaching of lead into the environment could still be problematic.[19–21] Alternative, non-toxic B-site cations are therefore an important avenue of investigation. The most commonly attempted substitution includes tin, which has been demonstrated to be less efficient, less stable, and more toxic than the lead analogue.[22,23] Other examined options for lead replacement include germanium, or the formation of 'double-perovskites' using elements such as bismuth or silver – yet the efficiency is still lower than lead-based counterparts.[24,25] Computational studies have suggested a range of potential lead-replacements that will enable high efficiency. Examples of elements that could be used are iron, manganese, zinc, calcium and magnesium.[26–29] Using these elements would maintain the advantages of the relative abundance and low cost from the lead-halide perovskites.[30] Crucially metal halide compounds using these elements are not highly harmful to the environment or to the scientist based on materials safety documentation.

[a] Department of Materials, Loughborough University, Loughborough, LE11 3TU, UK. E-mail: s.r.pering@lboro.ac.uk
[b] Loughborough Materials Characterisation Centre, Loughborough University, Loughborough, LE11 3TU, UK
[c] Centre for Renewable Energy Systems Technology, Loughborough University, Loughborough, LE11 3TU, UK

† Electronic supplementary information (ESI) available. See DOI: https://doi.org/10.1039/d2tc02582e

Table 1 Materials attempted during this study. Filled cells represent those not studied due to starting material safety documentation. References refer to computational analysis of potential materials

	Bromides			Iodides		
	K	Rb	MA	K	Rb	MA
Mg[26,28]						
Ca[28]	■	■	■			
Mn[26,28]				■	■	■
Fe[26]						
Cu[27,42]				■	■	■
Zn[26]	■	■	■			

Experimental examination of transition metal perovskite materials has yielded some initially promising results. Titanium and copper based perovskite materials have been successfully synthesised, with band gaps between 1.4 and 2.5 eV, demonstrating potential for solar cell application.[31–34] Cs_2TiBr_6 is one such example, a double perovskite with a 1.82 eV band gap, that can be used in a device to achieve 3.3% efficiency.[35] A-site cation rich perovskites based on copper-chloride produced a 2-D material with a band gap of 1.53 eV, and mixed-halide copper based perovskite solar cells have demonstrated photovoltaic activity.[36,37] Through solid-state synthesis of $(CH_3NH_3)_2CuX_4$, solar cells with efficiencies of over 2% could be fabricated.[34] Furthermore, as well as being employed as a dopant cation in MAPI, manganese has also been shown to exhibit some photovoltaic activity as a direct replacement for lead in methylamonnium manganese iodide.[38,39] There is therefore some promise to transition metal perovskite materials. Iron would be an ideal cation due to its abundance and low-cost. First-principles calculations suggest iron as a dopant cation in lead-based perovskites would improve the absorption coefficient.[40] However it was found that concentrations of iron in MAPI greater than at the ppm level greatly reduced the efficiency of the solar cell.[41] Using a smaller A-site cation such as potassium, computational measurements suggest that $KFeI_3$ could reach efficiencies of over 24%.[26] In this report the synthesis of a wide range of transition-metal based perovskite materials using a 1 : 1 ratio of A-site to B-site cation is attempted. A single, simple solution-based method is maintained throughout the report to ensure that candidate materials share the facile processing methods of their lead-containing counterparts, and all steps are carried out in air to ensure material stability in atmospheric conditions.

Results and discussion

Starting materials were chosen based on safety-documentation, *i.e.* only those that don't require special environmental measures or are toxic to wildlife were used throughout this examination. Table 1 displays all the combinations of materials studied, and will be updated throughout the report to display the progress of the materials through each of the screening stages. Throughout the report materials will be referred to as $AX:BX_2$ as exact confirmation of crystal structure was unobtainable.

The experimental screening of these materials will take part over 3 stages, as illustrated in Fig. 1: structural analysis using XRD, optical characterisation using UV/vis spectroscopy and finally *JV* curve analysis of completed devices. Only candidate materials which are deemed successful based on the criteria of the stage will move on to the next analysis stage. A single, simple solution based processing is used at each stage based on procedures developed for lead halide perovskites, both for consistency and to assess whether candidate materials share the beneficial solution processability of lead-based materials.

STAGE 1: to pass this stage, the synthesised material powders need to exhibit a PXRD pattern significantly different to the starting materials. As with computational screening, the first stage of the experimental screening procedure was to examine

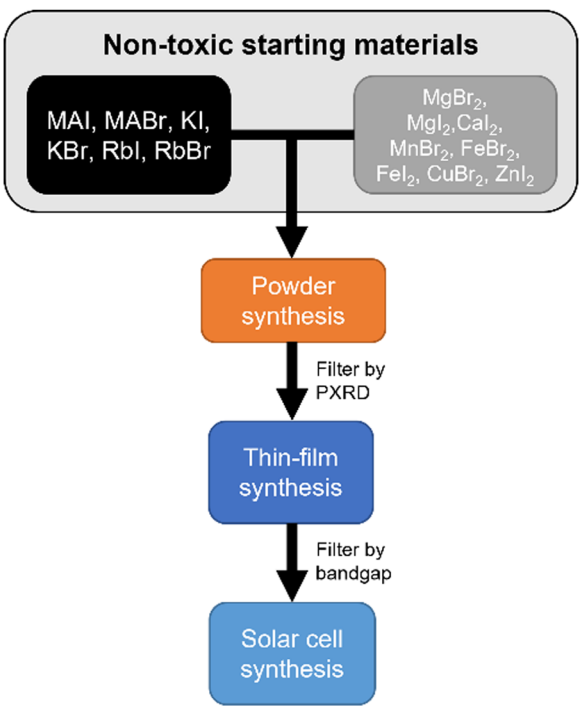

Fig. 1 Experimental screening procedure employed through this work.

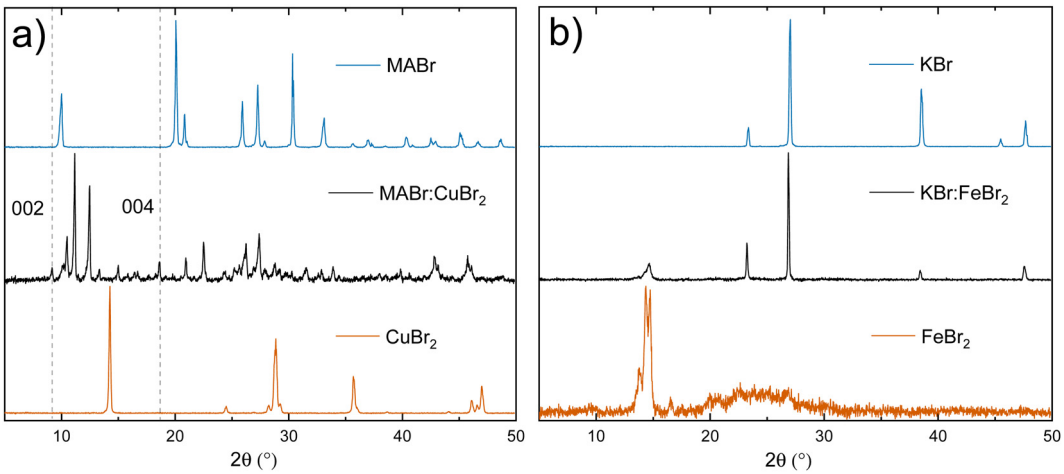

Fig. 2 Example normalised PXRD patterns of synthesised powders compared to starting material: (a) showing example of peaks not corresponding to starting materials and (b) showing no result through powder synthesis. Ref. 36 used to denote the reflections in (a).

the structure of the candidate materials. Powder synthesis was attempted for all 24 candidate materials using a 1 : 1 ratio of $AX:BX_2$ salt. Starting materials were dissolved in a solution of 7 : 3 GBL : DMSO[43] as an environmentally more benign alternative to DMF, before being cast into a glass Petri dish at 100 °C for one hour to evaporate the solvent. Candidate materials using magnesium as the sole B-site cation failed at this stage, with no viable powders formed to analyse through PXRD. Powders analysed through XRD were compared to their starting materials to observe if any new phases formed. Fig. 2 shows an example of a material deemed to have formed a new phase through PXRD (Fig. 2a) and a material that does not demonstrate any new peaks (Fig. 2 and Table 1b). All PXRD is displayed in the ESI.†

Starting with the calcium-based materials (Fig. S1, ESI†), peaks in all 3 synthesised powders at 2θ values of $\sim$13.4° and 15.8° are observed that cannot be attributed to the starting materials. The presence of CaI_2 and AI (where A is K, Rb or MA) peaks are noted in all samples, so there is incomplete conversion to a new phase. Single crystal data is not available in the literature to match these reflections. Two viable powders were formed using $MnBr_2$. $KBr:MnBr_2$ was hygroscopic and lost integrity before it could be analysed. The remaining powders (Fig. S2, ESI†) showed no un-matched peaks.

Red–orange-coloured powders could be formed using both iron bromide and iron iodide. While no new phases were detected through PXRD for any of the iodide containing samples (Fig. S3, ESI†), an unmatched peak in the $MABr:FeBr_2$ sample was detected at 17.2°. This was however a much smaller peak relative to the dominant MABr peak, showing that minimal conversion has taken place. Potassium and rubidium salts with iron bromide showed no new peaks in the XRD spectrum, suggesting no new materials have been made in these cases.

The remaining two transition metal candidates, copper and zinc, led to the formation of powders in all cases. For copper (Fig. S1a and S5, ESI†) the dark blue powders exhibited un-matched peaks in the region of 10–12° – in the case of $MABr:CuBr_2$ these are the dominant peaks. However, these more closely align with the non-perovskite peaks observed by Cortecchia *et al.* who synthesised copper perovskite powders using ethanol as the solvent.[44] Peaks at $\sim$9° and 17° 2θ assigned to the perovskite phase in the above work and the single crystal analysis by Elattar *et al.*[36] are also observed, although these are much less intense refractions. However, peaks corresponding to starting materials are still observed in all copper samples. Zinc iodide powders synthesised through stage 1 were an off-white colour. The 102 ZnI_2 peak at 25° was the dominant peak in all cases, with some unmatched peaks at 2θ values $<20°$.[45] Previously synthesised zinc based materials such as MA_2ZnCl_4 do not show the same structure as most perovskites, metal halide tetrahedra are formed as opposed to

Table 2 Materials taken through to stage 2 highlighted in green. Candidate materials that did not pass stage 1 are highlighted in red

	Bromides			Iodides		
	K	Rb	MA	K	Rb	MA
Mg						
Ca						
Mn						
Fe						
Cu						
Zn						

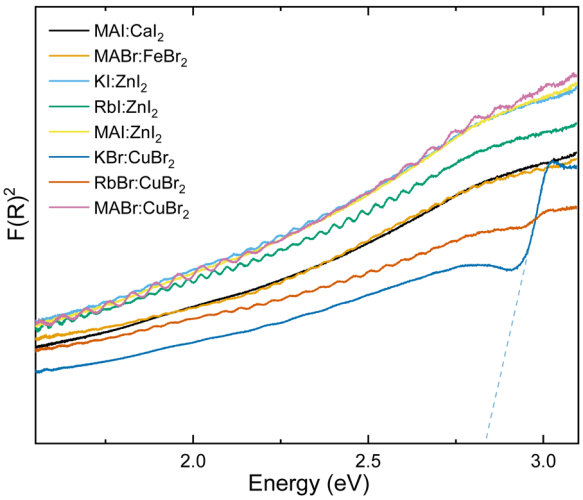

Fig. 3 Kubelka Munk analysis for thin-film materials in stage 2 analysis. Dashed lines show extrapolation to the *x*-axis for band gap identification.

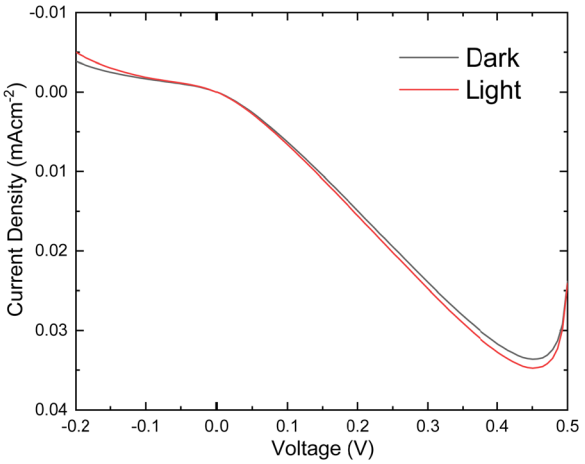

Fig. 4 A comparison of the dark and light *JV* curves for an example device. Measurements taken at 0.7 Sun.

octahedra found in materials such as $MAPbI_3$.[46] No powder/thin-film X-ray diffraction experiments have been performed on similar zinc materials, so it is not possible to determine whether the same structure has been made in these materials when using the much larger iodide ion.

Further analysis is required to fully characterise un-matched peaks in the diffractograms obtained through stage 1 of the experimental screening practice, and single-crystal analysis is an avenue for further research of any potentially suitable materials. The cause of the lack of viable formed phases is likely to be reaction with water or oxygen in the atmosphere, as for example the magnesium-based candidate materials could not be dried fully. For Samples that showed any un-matched peaks were used in stage 2 (displayed in Table 2).

Materials through to stage 2

STAGE 2: to pass this stage, the synthesised materials need to successfully form a thin-film and exhibit a band gap between 1.0 eV and 3 eV. Thin-films of the samples were cast from the same 1 molar solutions of 1 : 1 AX : BX_n samples in GBL : DMSO. A spin-coating speed of 2000 rpm was used for 20 seconds, then films were placed on a hotplate at 100 °C for one hour. Fig. S7 (ESI†) shows images for the thin-film attempts of calcium-based candidate materials compared to a blank microscope slide. While on the hot plate a thin film could be observed, upon removal from the heat the samples rapidly became transparent and liquid droplets were visible on the surface. While the powders themselves may have been stable enough to atmospheric conditions for PXRD measurements, the thin films were less resilient towards water ingress. Calcium based candidate materials with potassium and rubidium were ruled out of further analysis at this point. MAI:CaI_2 was stable enough to be analysed through UV/vis (Fig. 3 and Fig. S10, ESI†). Due to the low thickness and coverage of the thin-film the reflectance spectroscopy shows interference and no obvious band gap. This result fits with computational predictions for calcium perovskite band gaps using Cs^+ and Rb^+ as the A-site cation which exceed usable wavelengths for solar cells.[26,28] Thin-films of $MAFeBr_3$ and Zn based candidate materials showed a similar response, with high-transparency thin-films that do not possess an observable band gap within the usable range for photovoltaics. While computational calculations for iron-based perovskites predicted a band gap of 2.7 eV and therefore could have been observed in the experiment – zinc perovskite band gap predictions lie below 1 eV.[26,28]

Fig. 3 shows that only one of the 10 materials that passed stage 1 has an observable band gap, also illustrated in Table 3. For KBr:CuBr a band gap of 2.82 eV is measured, which is significantly larger than is predicted for the similar material $RbCuBr_3$, of 0.45 eV.[26] Furthermore the band gap for this material is significantly higher than the ideal band gap for

Table 3 Materials through to stage 3 in green; red, failed at stage 1, orange, failed at stage 2

	Bromides			Iodides		
	K	Rb	MA	K	Rb	MA
Mg						
Ca						
Mn						
Fe						
Cu	2.82 eV					
Zn						

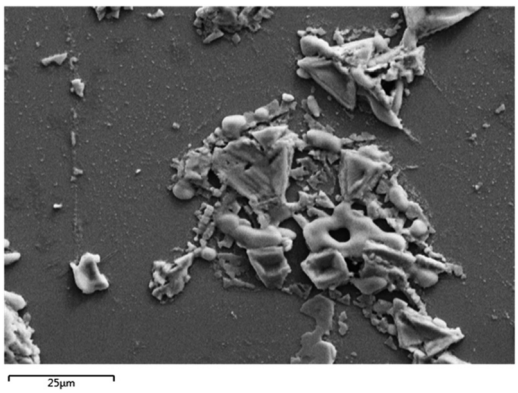

Fig. 5 SEM analysis of the KBr:$CuBr_2$ thin film.

maximum efficiency solar cells. While these results suggest that this non-toxic perovskite will not be suitable for traditional single-junction cells, their high transparency and larger band gap may be usable for multi-junction cells or building-integrated photovoltaic windows.

Materials through to stage 3

STAGE 3: solar cell synthesis. Only KBr:$CuBr_2$ possessed a band gap which may enable some photovoltaic activity. To test the performance, planar cells were fabricated using an inverted architecture: PEDOT:PSS as the hole-transport material and PCBM as the electron-transport material (dissolved in anisole as opposed to the more toxic toluene/chlorobenzene) were used to minimise the potential toxicity for the resulting devices. An image of the devices is shown in Fig. S10 (ESI†). Devices showed typical diode behaviour in the dark, however none showed any significant photovoltaic activity, as shown by an example device in Fig. 4. Voltage/current sweeps of all attempted devices are shown in Fig. S11 (ESI†). There was a large difference between the forward and reverse curves in each case, however given the performance of the devices it is difficult to assign this as hysteresis.

To explore possible effects of this poor performance, outside of the wide-band gap displayed, SEM images of the KBr:$CuBr_2$ film were analysed and shown in Fig. 5, with corresponding EDS analysis in Fig. S12 (ESI†). These images demonstrate significant phase-separation within the materials, with large crystals of copper and bromine, with minor integration of the A-site cation at other sites. While methylammonium copper halide materials have been successfully synthesised as solar cells and exhibit a 2D structure, the reduced size of potassium relative to methylammonium is likely to contribute to a change in structure, and potentially a reduction in the overall material viability.[44] There is also low overall coverage of the material, which is likely to be a significant contribution to the poor performance of the devices. Improving the morphology of the films is likely to be a difficult barrier to improving their photovoltaic performance and a source for future research. Alternatively mesoporous TiO_2 could be used as a framework for material deposition, which was used successfully by Elseman *et al.* to produce devices with >1% efficiency.[34]

Conclusions

A tabulated summary of the experimental screening process is shown in Table 4. The primary problem in the analysis of the non-toxic combinations was that in the majority of cases no viable material was formed; either no new product was made, or the material was rapidly unstable in atmospheric conditions. Future computational analysis to examine the stability of the hydrated structure with respect to the dry structure could predict problems with phase stability and suggest where controlled atmospheres are required. This could mean that more energy-intensive synthesis methods are required, reducing the beneficial properties of current perovskite solar cells, in that they are easy to manufacture.

The goal of this research was to assess combinations of non-toxic starting materials that had been identified as potential high-performance perovskite solar cell materials through computational calculations. None of the materials analysed through this study could be a suitable replacement for lead in a fully-non toxic material when aiming to maintain the same manufacturing processes as those used for lead-based compounds. Altering the solvent mixture, deposition time or using solid-state methods that have demonstrated successful devices could be a more appropriate avenue for further lead-free compound research. Mesoporous device structures would be of particular interest, as these could overcome the morphology problems, and have already been demonstrated to exhibit a reasonable efficiency.

Table 4 Summary of results, including champion cell efficiency for each successful material: Red indicates end at stage 1 (structural), orange at stage 2 (optical, No O-BG stands for No Observable Band Gap) and green signifies solar cell efficiency (stage 3, photovoltaics)

	Bromides			Iodides		
	K	Rb	MA	K	Rb	MA
Mg	Hygroscopic, no successful powder synthesis					
Ca				Hygroscopic films		
Mn	No powder	No new peaks				
Fe	No new peaks		No O-BG	No new peaks		
Cu	0 %	No O-BG	No O-BG			
Zn				No Observable Band Gap		

Author contributions

S. R. P.: conceptualisation, funding acquisition, project administration, methodology, supervision, writing – original draft. H. G., T. K., W. Z., K. Y. & M. T. data curation, formal analysis, investigation, resources and writing – review and editing.

Conflicts of interest

There are no conflicts to declare.

Acknowledgements

S. R. P. thanks Loughborough University for funding.

References

1 A. Kojima, K. Teshima, Y. Shirai and T. Miyasaka, *J. Am. Chem. Soc.*, 2009, **131**, 6050–6051.
2 J. Burschka, N. Pellet, S.-J. Moon, R. Humphry-Baker, P. Gao, M. K. Nazeeruddin and M. Grätzel, *Nature*, 2013, **499**, 316–319.
3 N. K. Noel, S. N. Habisreutinger, B. Wenger, M. T. Klug, M. T. Horantner, M. B. Johnston, R. J. Nicholas, D. T. Moore and H. J. Snaith, *Energy Environ. Sci.*, 2017, **10**, 145–152.
4 L. Chao, L. Pengwei, G. Hao, Z. Yiqiang, L. Fengyu, S. Yanlin, S. Guosheng, M. Nripan and X. Guichuan, *Sol. RRL*, 2018, **2**, 1700217.
5 K. Hwang, Y. S. Jung, Y. J. Heo, F. H. Scholes, S. E. Watkins, J. Subbiah, D. J. Jones, D. Y. Kim and D. Vak, *Adv. Mater.*, 2015, **27**, 1241–1247.
6 J. H. Noh, S. H. Im, J. H. Heo, T. N. Mandal and S. Il Seok, *Nano Lett.*, 2013, **13**, 1764–1769.
7 M. Saliba, T. Matsui, K. Domanski, J.-Y. Seo, A. Ummadisingu, S. M. Zakeeruddin, J.-P. Correa-Baena, W. R. Tress, A. Abate, A. Hagfeldt and M. Grätzel, *Science*, 2016, **354**, 206–209.
8 N. De Marco, H. Zhou, Q. Chen, P. Sun, Z. Liu, L. Meng, E.-P. Yao, Y. Liu, A. Schiffer and Y. Yang, *Nano Lett.*, 2016, **16**, 1009–1016.
9 A. Mahapatra, R. Runjhun, J. Nawrocki, J. Lewiński, A. Kalam, P. Kumar, S. Trivedi, M. M. Tavakoli, D. Prochowicz and P. Yadav, *Phys. Chem. Chem. Phys.*, 2020, **22**, 11467–11473.
10 S. R. Pering, W. Deng, J. R. Troughton, P. S. Kubiak, D. Ghosh, R. G. Niemann, F. Brivio, F. E. Jeffrey, A. B. Walker, M. S. Islam, T. M. Watson, P. R. Raithby, A. L. Johnson, S. E. Lewis and P. J. Cameron, *J. Mater. Chem. A*, 2017, **5**, 20658–20665.
11 G. Grancini, C. Roldán-Carmona, I. Zimmermann, E. Mosconi, X. Lee, D. Martineau, S. Narbey, F. Ostwald, F. De Angelis, M. Graetzel and M. K. Nazeeruddin, *Nat. Commun.*, 2017, **8**, 15684.
12 F. Ansari, E. Shirzadi, M. Salavati-Niasari, T. LaGrange, K. Nonomura, J.-H. Yum, K. Sivula, S. M. Zakeeruddin, M. K. Nazeeruddin, M. Grätzel, P. J. Dyson and A. Hagfeldt, *J. Am. Chem. Soc.*, 2020, **142**, 11428–11433.
13 J. Azadmanjiri, J. Wang, C. C. Berndt and A. Yu, *J. Mater. Chem. A*, 2018, 3824–3849.
14 X. Zhang, G. Wu, W. Fu, M. Qin, W. Yang, J. Yan, Z. Zhang, X. Lu and H. Chen, *Adv. Energy Mater.*, 2018, **8**, 1702498.
15 M. A. Green, E. D. Dunlop, J. Hohl-Ebinger, M. Yoshita, N. Kopidakis and A. W. Y. Ho-Baillie, *Prog. Photovoltaics Res. Appl.*, 2020, **28**, 3–15.
16 Y. Y. Zhang, S. Chen, P. Xu, H. Xiang, X. G. Gong, A. Walsh and S. H. Wei, *Chin. Phys. Lett.*, 2018, **35**, 036104.
17 C. Tian, E. Castro, T. Wang, G. Betancourt-Solis, G. Rodriguez and L. Echegoyen, *ACS Appl. Mater. Interfaces*, 2016, **8**, 31426–31432.
18 J. Li, H.-L. Cao, W.-B. Jiao, Q. Wang, M. Wei, I. Cantone, J. Lü and A. Abate, *Nat. Commun.*, 2020, **11**, 310.
19 P. Su, Y. Liu, J. Zhang, C. Chen, B. Yang, C. Zhang and X. Zhao, *J. Phys. Chem. Lett.*, 2020, **11**, 2812–2817.
20 Y. Zhai, Z. Wang, G. Wang, W. J. G. M. Peijnenburg and M. G. Vijver, *Chemosphere*, 2020, **249**, 126564.
21 F. Schmidt, L. Ledermann, A. Schäffer, H. J. Snaith and M. Lenz, *J. Hazard. Mater.*, 2022, **436**, 128995.
22 N. K. Noel, S. D. Stranks, A. Abate, C. Wehrenfennig, S. Guarnera, A.-A. Haghighirad, A. Sadhanala, G. E. Eperon, S. K. Pathak, M. B. Johnston, A. Petrozza, L. M. Herz and H. J. Snaith, *Energy Environ. Sci.*, 2014, **7**, 3061–3068.
23 A. Babayigit, D. Duy Thanh, A. Ethirajan, J. Manca, M. Muller, H.-G. Boyen and B. Conings, *Sci. Rep.*, 2016, **6**, 18721.
24 I. Kopacic, B. Friesenbichler, S. F. Hoefler, B. Kunert, H. Plank, T. Rath and G. Trimmel, *ACS Appl. Energy Mater.*, 2018, **1**, 343–347.
25 A. H. Slavney, T. Hu, A. M. Lindenberg and H. I. Karunadasa, *J. Am. Chem. Soc.*, 2016, **138**, 2138–2141.
26 R. Jacobs, G. Luo and D. Morgan, *Adv. Funct. Mater.*, 2019, **29**, 1804354.
27 T. Nakajima and K. Sawada, *J. Phys. Chem. Lett.*, 2017, **8**, 4826–4831.
28 M. R. Filip and F. Giustino, *J. Phys. Chem. C*, 2016, **120**, 166–173.
29 H. Sabzyan and F. Ghaderi, *Mater. Today Commun.*, 2021, **26**, 101847.
30 H. J. Snaith, *J. Phys. Chem. Lett.*, 2013, **4**, 3623–3630.
31 D. Kong, D. Cheng, X. Wang, K. Zhang, H. Wang, K. Liu, H. Li, X. Sheng and L. Yin, *J. Mater. Chem. C*, 2020, **8**, 1591–1597.
32 X.-L. Li, Z. Li, G. Zhang and G.-J. Yang, *J. Mater. Chem. A*, 2020, **8**, 5484–5488.
33 W. Li, S. Zhu, Y. Zhao and Y. Qiu, *J. Solid State Chem.*, 2020, **284**, 121213.
34 A. M. Elseman, A. E. Shalan, S. Sajid, M. M. Rashad, A. M. Hassan and M. Li, *ACS Appl. Mater. Interfaces*, 2018, **10**, 11699–11707.
35 M. Chen, M.-G. Ju, A. D. Carl, Y. Zong, R. L. Grimm, J. Gu, X. C. Zeng, Y. Zhou and N. P. Padture, *Joule*, 2018, **2**, 558–570.
36 A. Elattar, W. Li, H. Suzuki, T. Kambe, T. Nishikawa, A. K. K. Kyaw and Y. Hayashi, *Chem. – Eur. J.*, 2022, **28**, e202104316.

37 K. Ahmad, P. Kumar, H. Kim and S. M. Mobin, *ChemNanoMat*, 2022, **8**, e202200061.
38 W. Liu, L. Chu, N. Liu, Y. Ma, R. Hu, Y. Weng, H. Li, J. Zhang, X. Li and W. Huang, *J. Mater. Chem. C*, 2019, **7**, 11943–11952.
39 X. Zhang, J. Yin, Z. Nie, Q. Zhang, N. Sui, B. Chen, Y. Zhang, K. Qu, J. Zhao and H. Zhou, *RSC Adv.*, 2017, **7**, 37419–37425.
40 L. Zhou, J. Chang, Z. Lin, C. Zhang, D. Chen, J. Zhang and Y. Hao, *RSC Adv.*, 2017, **7**, 54586–54593.
41 J. R. Poindexter, R. L. Z. Hoye, L. Nienhaus, R. C. Kurchin, A. E. Morishige, E. E. Looney, A. Osherov, J.-P. Correa-Baena, B. Lai, V. Bulović, V. Stevanović, M. G. Bawendi and T. Buonassisi, *ACS Nano*, 2017, **11**, 7101–7109.
42 F. Akrout, F. Hajlaoui, K. Karoui, N. Audebrand, T. Roisnel and N. Zouari, *J. Solid State Chem.*, 2020, **287**, 121338.
43 S. N. Manjunatha, Y.-X. Chu, M.-J. Jeng and L.-B. Chang, *J. Electron. Mater.*, 2020, **49**, 6823–6828.
44 D. Cortecchia, H. A. Dewi, J. Yin, A. Bruno, S. Chen, T. Baikie, P. P. Boix, M. Grätzel, S. Mhaisalkar, C. Soci and N. Mathews, *Inorg. Chem.*, 2016, **55**, 1044–1052.
45 P. Tyagi and A. G. Vedeshwar, *Phys. Rev. B: Condens. Matter Mater. Phys.*, 2001, **64**, 245406.
46 B. Morosin and K. Emerson, *Acta Crystallogr., Sect. B: Struct. Crystallogr. Cryst. Chem.*, 1976, **32**, 294–295.

